RSC Advances

PAPER

View Article Online
View Journal | View Issue

Cite this: *RSC Adv.*, 2017, **7**, 43888

Fabrication of rGO/g-C_3N_4 composites *via* electrostatic assembly towards charge separation control

Xiao Zhang,*[a] Changchao Jia,[b] Yuehua Xue[a] and Ping Yang *[b]

Received 13th July 2017
Accepted 25th August 2017

DOI: 10.1039/c7ra07706h

rsc.li/rsc-advances

Herein, g-C_3N_4 nanosheets (NSs) were grown on reduced graphene oxide (rGO) using cross linking molecules by an electrostatic assembly process from carboxyl and amine groups *via* π–π stacking interaction to fabricate heterostructures. Detailed characterizations such as Fourier transform infrared spectroscopy, transmission electron microscopy, scanning electronmicroscopy, photoelectrochemical measurements, X-ray photoelectron spectroscopy, and photoluminescence (PL) spectroscopy demonstrated step-by-step immobilization of 1-pyrene carboxylic acid, polyaniline (PANI), and g-C_3N_4 on rGO. The π–π stacking plays an important role for the formation of rGO/g-C_3N_4 composites. The surface of rGO was homogeneously decorated with monodispersed g-C_3N_4 NSs. The resulting rGO/g-C_3N_4 composites obtained endowed the heterostructures with novel functions. Both the rGO–COOH/g-C_3N_4 and rGO–PANI/g-C_3N_4 composites revealed enhanced conduction properties. Absorption and PL spectra of the composite samples confirmed the attachment of g-C_3N_4 on rGO. Due to the presence of carboxyl groups on 1-pyrene carboxylic acid, rGO–COOH/g-C_3N_4 composites demonstrated enhanced photocatalysis properties.

Introduction

When the development of single functional materials no longer satisfies the demands of material fabrication applications, harmonization and combination of various effects and factors are always the key to the construction of novel nanomaterials for functional development. Nanoarchitectonics has been proposed as a novel concept in nanofabrication.[1] The development of highly sophisticated multifunctional nanomaterials by coupling and combining single functional nanomaterials and monotonous nanostructures has become a trend in nanomaterial fabrication.[2] Graphene, with its excellent conductivity, good transparency and extremely high surface to volume ratio,[3–8] is one of the most popular and reliable carbon-based materials in current times. Its unique electronic properties and highly transparent one atom thick layer provides possibility for constructing graphene-based nanoarchitectured materials (*e.g.* semiconducting composite materials, insulating materials) *via* chemical modification on its surface.[3]

Recently, polymeric graphitic carbon nitride (g-C_3N_4) has become a promising material for various applications owing to its narrow bandgap for visible light absorption, low cost, proper electronic structure and high thermal and chemical stability.[4–7] As an environment and economic friendly metal-free carbon-based nanomaterial, g-C_3N_4 is another rising star in the photocatalysis-driven energy production field due to its excellent chemical stability and inert nature. With its narrow band gap of 2.7 eV, C_3N_4 has successfully captured people's attention. C_3N_4, coupled and combined with other nanomaterials, could be used as visible-light induced semiconductor photocatalyst for organic chemical degradation and watersplitting.[7,9–12] However, one of the disadvantages of C_3N_4 only/polymeric g-C_3N_4 is the limited separation efficiency of the photogenerated electron–hole pairs.[13] Thus, the formation of heterojunction has attracted great attention for improving the carriers' separation efficiency and reaction stability as well as for constructing complex systems.

Intermolecular interactions such as hydrogen bonding, metal coordination and dipolar coupling have been used for spontaneous association of molecules into stable aggregates with well-defined architectures.[14] In comparison to the covalent modification that causes disruption of the conjugated structure of the graphene sheets, π–π stacking and other non-covalent methods are usually preferred when graphene sheets' electronic properties and large surface to volume ratio are required. One significant advantage of π–π stacking interaction is that the bonding strength could approach that observed due to covalent modifications.

Polyaniline (PANI), as a conducting polymer, has unique charge transport properties.[13] rGO-based PANI composites and combinations of rGO with other semiconductor materials have

[a]*School of Chemistry, University of New South Wales, Sydney 2052, Australia. E-mail: xiao.zhang2@student.unsw.edu.au*

[b]*School of Material Science and Engineering, University of Jinan, Nanxinzhuangxi RD, 336, Jinan, 250022, P. R. China. E-mail: mse_yangp@ujn.edu.cn*

been discovered. Most of these studies have been focused on developing photocatalytic materials using PANI in combination with other semiconductors. Wei *et al.* reported PANI–TiO_2 composites exhibiting enhanced photocatalytic acetone degradation activity.[15,16] However, very few reports focused on the synthesis and study of the photoactivity of the rGO–PANI/g-C_3N_4 composites system. Thus, to improve the property of rGO and C_3N_4 based nanomaterials, herein, we are following the idea of nanoarchitectonics by combining reduced graphene oxide (rGO), g-C_3N_4 nanosheets (NSs) with PANI (a popular conducting polymer with excellent chemical stability) and 1-pyrene carboxylic acid using the idea of π–π stacking interaction. In this study, we aim to introduce rGO–pyrene–PANI/g-C_3N_4 (rGO–COOH–PANI/g-C_3N_4) composites nanomaterials using the idea of nanoarchitetonics and π–π stacking interaction based bonding systems towards property control and the mechanism elucidation. Detailed characterization of the samples demonstrated step-by-step assembly of 1-pyrene carboxylic acid, PANI, and g-C_3N_4. π–π stacking interaction is an important driving force that enables the formation of rGO/g-C_3N_4 composites exhibiting homogeneous and monodispersed structures.

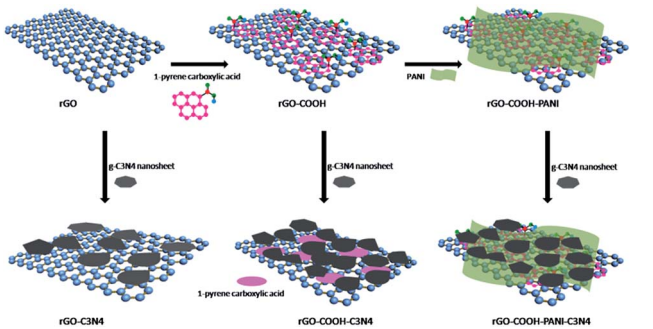

Scheme 1 Attachment of g-C_3N_4 NSs on rGO to form heterostructures with three approaches: (left) direct attachment of g-C_3N_4 NSs on rGO; (middle) attachment of g-C_3N_4 NSs on rGO-based 1-pyrene carboxylic acid composites; (right), immobilization using 1-pyrene carboxylic acid and PANI as linker molecules.

Experimental

Chemicals

All chemicals *e.g.* sodium nitrite ($NaNO_2$), potassium permanganate ($KMnO_4$), sulfuric acid (98%), HCl, hydrogen peroxide (30% w/w), sodium borohydride, 1-pyrene carboxylic acid, PANI, and dimethylformamide (DMF) were purchased from Sigma Aldrich. All chemicals and solvents were used directly as received.

Preparation of samples

A modified Hummers' method was used for the synthesis of graphene oxide (GO).[17] rGO was obtained by reduction of GO using sodium borohydride. Graphene oxide and sodium borohyrdride were mixed with constant stirring followed by sonication. The resulting solution was then heated to 90 °C for 1 h with stirring. For the preparation of g-C_3N_4 NSs, a slightly modified method from Liu *et al.* (2016) was used.[18] Bulk g-C_3N_4 was treated with a solution containing a mixture of concentrated sulfuric acid (H_2SO_4) and nitric acid (HNO_3) at room temperature to obtain porous g-C_3N_4. The porous g-C_3N_4 was then dispersed into a concentrated $NH_3 \cdot H_2O$ solution with 1 h of stirring followed by a heat-treatment process in a Teflon-lined stainless steel autoclave at 180 °C to obtain g-C_3N_4 NSs.

The process of g-C_3N_4 NSs decoration on rGO was carried out using 1-pyrene carboxylic acid or/and PANI as the linker. An assembly process *via* π–π stacking was used to fabricate rGO–PANI/g-C_3N_4 composite heterostructures. Initially, 1-pyrene carboxylic acid was π–π stacked onto rGO by mixing rGO with excess of 1-pyrene carboxylic acid in ethanol solution followed by sonication and filtration with millipore PVDF membrane to prepare rGO–COOH. Scheme 1 shows the assembly process of rGO/g-C_3N_4 heterostructures. The attachment of PANI and g-C_3N_4 was carried out as follows: rGO-based PANI and 1-pyrene carboxylic acid composite samples were dispersed in DMF in individual solutions. The two solutions were then mixed in a volume ratio of 1 : 4 to prepare the rGO–COOH–PANI sample. To investigate the effect of –COOH and PANI on the properties of the resulting samples, 40 mL dispersions of rGO, rGO–COOH and rGO–COOH–PANI were individually mixed with 3 mL of g-C_3N_4 NSs solution, followed by sonication for 30 min to prepare rGO-g-C_3N_4, rGO–COOH–g-C_3N_4, and rGO–COOH–PANI–g-C_3N_4 samples, respectively.

Instrumentation

Scanning electron microscopy (SEM) images of the samples were obtained using field-emission scanning electron microscope (QUANTA 250 FEG, FEI, USA). Transmission electron microscopy (TEM) images were obtained using a JEOL-2100 microscope under an acceleration voltage of 200 kV and high-resolution transmission electron microscopy (HRTEM) was recorded using a transmission electron microscope (FEI Tecani F20 TEM). Raman spectra were obtained using a high-resolution Raman spectrometer (LabRAM HR Evolution, HORIBA JOBIN YVON SAS). Fourier transform infrared (FTIR) spectra of the samples were recorded using a Fourier infrared spectrometer (Thermo Electron, Nicolet380, United States). X-ray photoelectron spectroscopy (XPS) was carried out using a Thermo Fisher Scientific Escalab 250 spectrometer.

UV/Vis absorption and photoluminescence (PL) spectra (excitation and emission slit width: 2.5 nm) were recorded using a conventional UV/Vis spectrometer (Hitachi U-4100) and a fluorescence spectrometer (Hitachi F-4600). Chi660e electrochemical analyzer (Chen Hua Instruments, Shanghai) in a standard three-electrode cell (in which Pt sheet functionalized as counter electrode; Ag/AgCl as the reference electrode; and sodium sulfate aqueous solution (1 mol L^{-1}) as electrolyte) was used for measurement of photocurrent. A thin film of each of the sample solutions was casted on the indium tin oxide (ITO) glass surface (working electrode) with an active area of 4 cm^2. A 300 W xenon lamp was used as the light source. The photocatalytic activity of the as-synthesized samples was evaluated by degradation of Rhodamine B (RhB) using a 300 W Xe lamp

under visible light irradiation. Typically, 10 mg of the samples were added to each of the 25 mL (10 mg L^{-1}) RhB aqueous solution for photocatalysis measurements.

Results and discussion

Fig. 1 shows the SEM images of GO and rGO samples. The figure shows that the GO and rGO samples are wrinkled sheets with high transparency resulting from the deformation and distortion of graphite sheets during the oxidation and reduction process. g-C_3N_4 NSs of several tens of nanometers were fabricated using the method reported in the literature.[18]

As illustrated in Scheme 1, g-C_3N_4 NSs were immobilized on rGO using three approaches for comparison. As for sample rGO–COOH–PANI/g-C_3N_4, 1-pyrene carboxylic acid was π–π stacked onto rGO surface to obtain –COOH decorated rGO (rGO–COOH) followed by attachment of PANI on rGO–COOH *via* chemical bonding to form the rGO–COOH–PANI composite material. Finally, C_3N_4 NSs were decorated onto rGO–COOH–PANI *via* π–π stacking. Fig. 2 shows the TEM images of the rGO/g-C_3N_4 and rGO–COOH–PANI/g-C_3N_4 samples. The inset in Fig. 2d shows the profile of lattice fringes of C_3N_4 NSs. The interplanar spacing of the NSs is clearly observed and matched that of the C_3N_4, which confirms the tight assembly of NSs on the surface.

In the case of direct immobilization of C_3N_4 NSs on rGO without using cross linking molecules (sample rGO/g-C_3N_4 in Fig. 2a and b), aggregation of C_3N_4 NSs could be observed on the surface of rGO. A lower degree of agglomeration of C_3N_4 NSs was observed for samples in which 1-pyrene carboxylic acid was used as the linker. It was demonstrated that C_3N_4 NSs are homogeneously distributed on the composite material surface after deposition of PANI as shown in Fig. 2c and d. Differences in PL intensity of the NSs were observed for the rGO/g-C_3N_4 and rGO–COOH–PANI/g-C_3N_4 samples as compared to the initial C_3N_4 NSs sample. Enhanced PL property was observed for rGO–COOH–/g-C_3N_4 sample due to the fact that carboxyl groups on the surface could be electrostatically adsorbed onto the surface of C_3N_4 NSs to passivate surface defects, which also confirms the successful assembly of NSs on rGO.

Fig. 3 shows the FTIR spectra of rGO/g-C_3N_4, rGO–COOH/g-C_3N_4, and rGO–COOH–PANI/g-C_3N_4 samples, which further confirm the assembly of 1-pyrene carboxylic acid, PANI, and

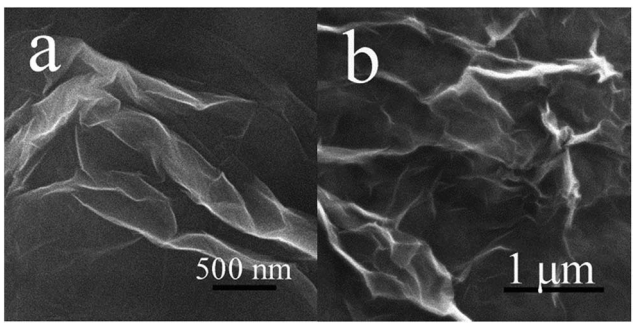

Fig. 1 SEM images of samples. (a), GO. (b), rGO.

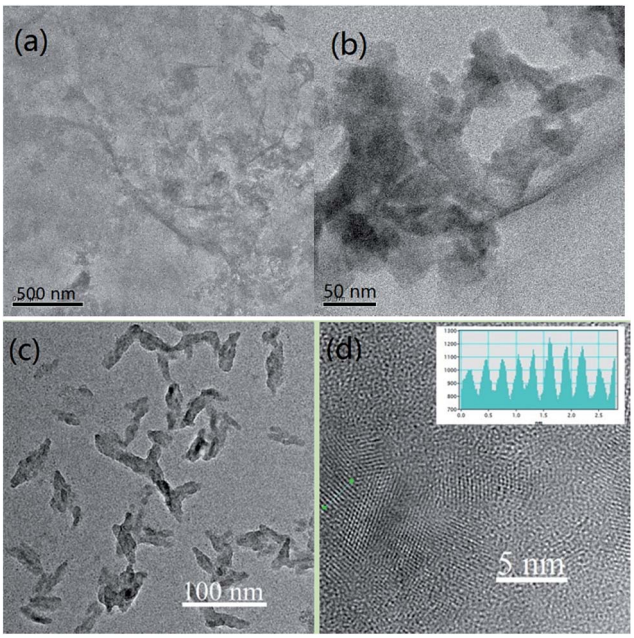

Fig. 2 TEM images of samples. (a & b) rGO/g-C_3N_4. (c & d) rGO–COOH–PANI/g-C_3N_4. Inset in (d) shows the profile of lattice fringes of g-C_3N_4 NSs.

C_3N_4 NSs on the rGO surface. The FTIR spectrum of rGO–COOH–PANI/g-C_3N_4 sample displays prominent peaks at 3438, 2918, 2850, 1575, 1490, 1370, 1032, and 800 cm^{-1}, corresponding to –OH, –C–H, –$(C–H)_n$,–C═N, –C═C –C–N, –N–H, and –C–H stretching vibrations, respectively. These peaks are attributed to the presence of rGO, 1-pyrene carboxylic acid, PANI, and C_3N_4. The –C═O stretching vibration at 1723 cm^{-1} is observed (red line) in the 1-pyrene carboxylic acid assembled sample. The black line in Fig. 3 confirms the presence of rGO and g-C_3N_4 in the sample. Compared with the FTIR spectrum of the rGO–COOH–g-C_3N_4 sample, several additional peaks at 1575, 1490, 1370, 1032, and 800 cm^{-1} corresponding to the stretching vibrations of –C═N, –C═C, –C–N, –N–H, and –C–H in PANI are observed in the spectrum of the rGO–COOH–PANI/g-C_3N_4 sample. These peaks confirm the combination of PANI with rGO.

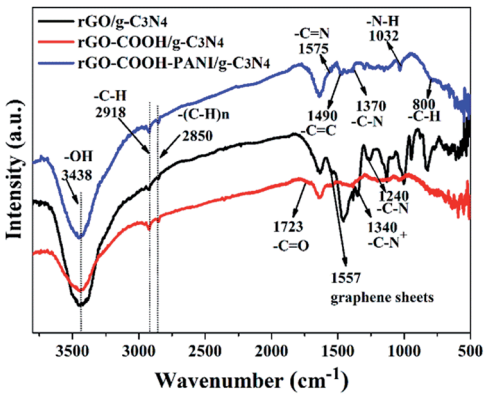

Fig. 3 FTIR spectra of the rGO/g-C_3N_4, rGO–COOH/g-C_3N_4, and rGO–COOH–PANI/g-C_3N_4 samples.

XPS analysis confirms the formation of rGO-C_3N_4 heterostructures using 1-pyrene carboxylic acid and PANI as linkers. It was demonstrated that the main elements on the surface of the samples are carbon and nitrogen with limited amounts of adsorbed oxygen. These O atoms are ascribed to the –COOH groups. Fig. 4 shows the high-resolution XPS spectra of the rGO–COOH/g-C_3N_4 and rGO–COOH–PANI/g-C_3N_4 samples. The photoelectron peaks appear at binding energies of 284.8 (C 1s) and 399.8 eV (N 1s). The photoelectron signal of C 1s has two distinct peaks around 284 and 286 eV that are attributed to the graphitic carbon adsorbed on the surface as well as carbon species from 1-pyrene carboxylic acid and PANI.[3,9] In addition, the XPS signal for the carbon atoms bonded to three nitrogen atoms in the g-C_3N_4 lattice occurs at about 288 eV.[18] The high resolution N 1s XPS spectra shown in Fig. 4b and d also have two distinct peaks, in the range of binding energies from 399.9 to 402 eV (for both the rGO–COOH/g-C_3N_4 and rGO–COOH–PANI/g-C_3N_4 samples). This indicates the co-existence of a number of distinguishable nitrogen environments. The two peaks could be assigned to tertiary nitrogen (N–$(C)_3$) and to the N atoms that are sp^2-bonded to two carbon atoms (C–N=C).[19] This confirms the presence of graphite-like sp^2-bonded graphitic carbon nitride. Furthermore, the intensity of the peak at 402 eV increased on addition of PANI. Fig. 5 shows the Raman spectra of the samples with D band at 1342 cm^{-1}, G band at 1600 cm^{-1}, 2D band at 2700 cm^{-1}, and 3S peak at 2900 cm^{-1}. The band at 1168 cm^{-1} for sample rGO–COOH–PANI/g-C_3N_4 is ascribed to PANI, while the band at 466 cm^{-1} is ascribed to C_3N_4.

The band gap energy of composite materials depends strongly on their chemical composition.[20–23] Ge *et al.* have reported that the band gap of PANI is about 2.76 eV. The π-orbital and π*-orbital edge potentials are +0.62 eV and −2.14 eV, respectively. The edge potentials are well matched with the CB potential (−1.13 eV) and VB potential (+1.57 eV) of C_3N_4.[13] The excited state electrons produced by PANI are injected into the CB of the C_3N_4, while holes on the VB of C_3N_4 migrate to the

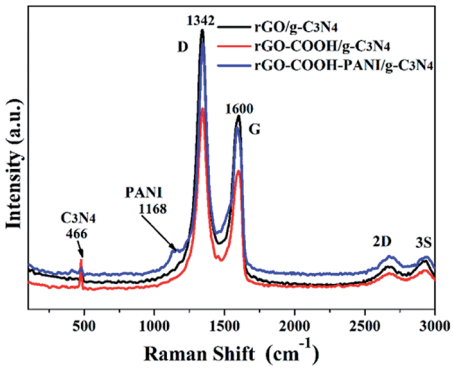

Fig. 5 Raman spectra of rGO/g-C_3N_4, rGO–COOH/g-C_3N_4 and rGO–COOH–PANI/g-C_3N_4 composite sample.

π-orbital of PANI. We investigated the absorption and PL of the samples (Fig. 6a and b) to demonstrate changes in their optical properties associated with their microstructures. Fig. 6a shows the absorption spectra of g-C_3N_4, rGO–COOH–PANI and their composites. The composites (sample rGO–COOH–PANI/g-C_3N_4) revealed enhanced absorption in the visible light region, which

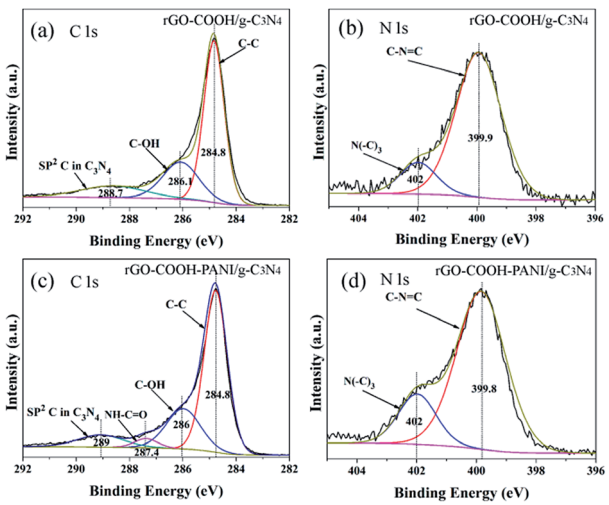

Fig. 4 High-resolution XPS spectra of rGO–COOH/g-C_3N_4 (a and b) and rGO–COOH–PANI/g-C_3N_4 (c and d). XPS spectra of C 1s (a and c). Spectra of N 1s (b and d).

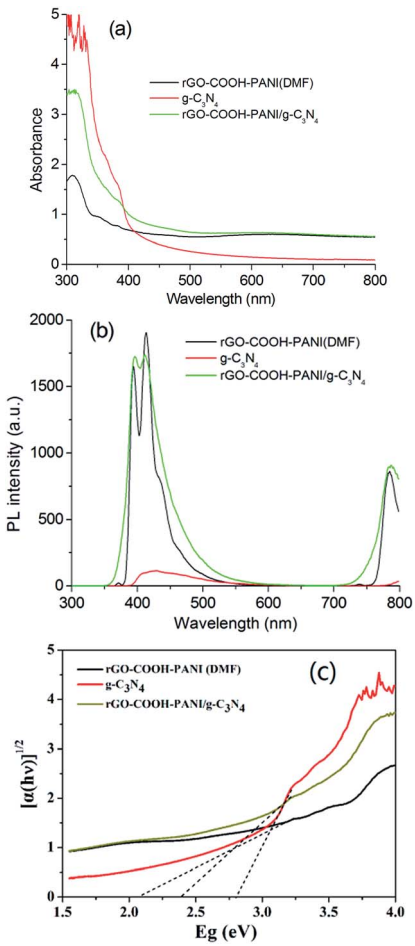

Fig. 6 (a) Absorption and (b) PL spectra of samples g-C_3N_4, rGO–COOH–PANI, and rGO–COOH–PAN/g-C_3N_4. (c) Band gaps of samples.

indicates changes in the band gap. According to the Kubelka–Munk function formula; $A(h\nu - E_g)^{1/2} = \alpha h\nu$, where α is the absorption coefficient, h is Plank's constant, ν is frequency, E_g is the band gap energy and A is a constant; the band gaps of 2.8 eV for g-C_3N_4 and 2.38 eV for rGO–COOH–PANI/g-C_3N_4 were clearly shown in Fig. 6c. Moreover, the PL intensity of the sample decreased after deposition of PANI owing to the interactions between rGO, PANI and g-C_3N_4 NSs. PANI, with its unique electronic properties and great chemical stability, is one of the most popular and most commonly used conducting polymers.[24,25] The decrease in PL intensity is ascribed to the charge transfer in the composites system including PANI which affects the PL process. To further confirm the formation of composite hetero-structures, the effect of composition on the photocurrent of the samples was investigated *via* *I–t* characteristics with chopped light, in which both dark current and photocurrent are generated during a single sweep. Pure g-C_3N_4 NSs and –COOH modified rGOs and PANI modified composite materials were investigated for comparison. Fig. 7 shows the transient photocurrent responses (*I–t*) for pure g-C_3N_4 and the other samples. Since photogenerated electrons migrated to the ITO substrates to produce photocurrent during visible light irradiation, rapid photocurrent value changes were observed when the lamp was switched on and off, in sequence.

As shown in Fig. 7 (a–c), all composite samples (rGO/g-C_3N_4, rGO–COOH/g-C_3N_4, and rGO–PANI/g-C_3N_4) revealed enhanced photocurrent generation. Generation of photocurrent and electron transfer in the system could be improved with increase in conductivity. Highly conductive molecules (*e.g.* 1-pyrene carboxylic acid) adsorbed onto a surface in a non-invasive fashion (π–π stacking interaction) enhances the conductivity of graphene-based materials. For the rGO-COOH/g-C_3N_4 sample, both π–π stacking interaction and chemical bonding interaction enhance the conductivity. PANI absorbs photons to induce π–π* transition, transporting the excited electrons to the π*-orbital.[13] When g-C_3N_4 NSs were attached onto the surface of PANI-modified rGO, the photocurrent was larger than that of the rGO/g-C_3N_4 (3.6 μA). This confirms the presence of the relatively strong interactions between g-C_3N_4 NSs and PANI. The conductivity of g-C_3N_4 is poor compared to that of PANI. However, their composites revealed rapid electron transfer in the composites system. Moreover, the dense g-C_3N_4 NSs layer could be formed on the PANI layer owing to the presence of rGO sheets. Thus, the excited state electrons produced by PANI were injected into the conduction band (CB) of the g-C_3N_4 with the holes on the VB of g-C_3N_4 migrating simultaneously to the π-orbital of PANI.[13] In addition, PANI, as a good hole conductor, is an electron donor upon photoexcitation. This phenomenon also supports the decrease in PL intensity of the rGO–COOH–PANI/g-C_3N_4 composites.

The photocatalytic activities of the as-prepared samples were investigated as shown in Fig. 8. Sample rGO/g-C_3N_4 revealed fast degradation rate while sample rGO–COOH/g-C_3N_4 revealed slow photocatalytic degradation for RhB. On completion of five cycles, the degradation rate of rGO–COOH/g-C_3N_4 remained at 90%. In contrast, almost no RhB degradation occurred in the

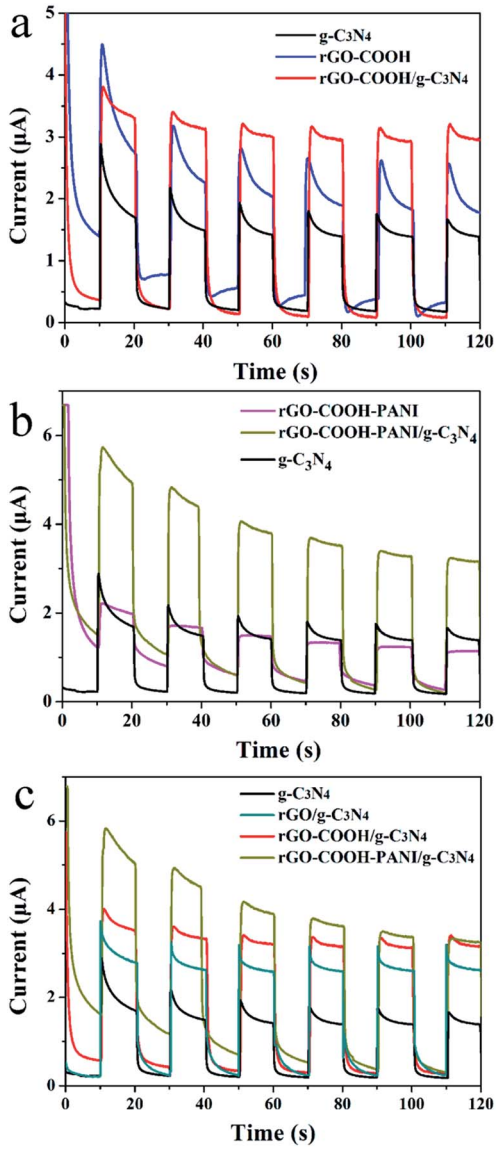

Fig. 7 (a–c) Transient photocurrent responses (*I–t*) for pure g-C_3N_4 NSs, rGO modified by –COOH and PANI as well as composites samples.

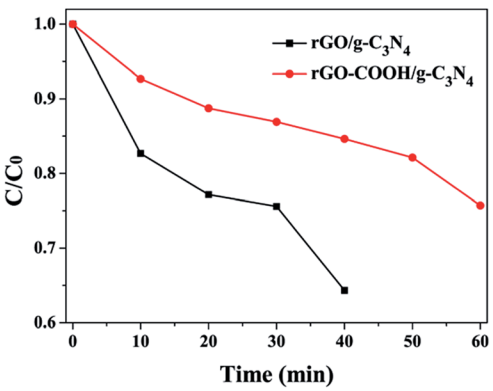

Fig. 8 Photocatalytic degradation of RhB under visible light irradiation for the rGO/g-C_3N_4 and rGO–COOH/g-C_3N_4 samples.

rGO–COOH–PANI/g-C_3N_4 sample. This confirms that charge separation occurred when rGO was connected to g-C_3N_4. In the case of –COOH groups as linkers, the charge separation is limited. This is due to the tight assembly of g-C_3N_4 NSs on the surface of rGO at the presence of 1-pyrene carboxylic acid as the linking molecule. Furthermore, a PANI layer restricts the charge separation for photocatalysis. However, the photocurrent response was enhanced in such composites as shown in Fig. 7. The PL intensity of this sample however increased compared with that of the pure g-C_3N_4 NSs sample. One way to explain this could be that the separation of the photogenerated carriers increased due to π–π* transition and that the surface defects of the NSs decreased at the presence of –COOH groups, and thus enhancing PL. In addition, rGO–COOH–PANI/g-C_3N_4 composites revealed poor photocatalysis activity, which differs from the reports shown in the literature. In the case of PANI–C_3N_4 without rGO, enhanced visible photocatalysis was observed.[13] Most possibly, this could be associated with the rGO layer which causes electrons migration in the system. We will investigate the mechanism in the near future. To confirm the stability of the composite samples, five cycles of visible light irradiation were run and analysed for the photocatalytic degradation of RhB. After continuous irradiation in each cycle, no significant loss in the photodegradation rate was observed, which confirms high stability of the composite.

Conclusions

Novel rGO–COOH–PANI/g-C_3N_4 composite heterostructures were fabricated *via* π–π stacking interaction and chemical bonding between carboxyl and amine groups. Detailed investigation demonstrated step-by-step assembly of 1-pyrene carboxylic acid, polyaniline, and g-C_3N_4. Such decorations endowed the heterostructures with novel characteristics, such as, enhanced photocurrent generation and rapid changes in PL intensity. The FT-IR and XPS spectra as well as TEM images confirmed the bonding interaction between rGO, PANI, and g-C_3N_4 NSs. rGO–COOH/g-C_3N_4 composite material revealed rapid photocatalytic degradation of RhB as compared to rGO/g-C_3N_4 without using 1-pyrene carboxylic acid as a linker molecule. The rGO–COOH–PANI/g-C_3N_4 sample revealed poor photocatalytic activity under visible light. This result is utilizable to understand the migration mechanism of electrons in nanoheterostructures modified by conducting molecules, such as 1-pyrene carboxylic acid in a noninvasive fashion.

Conflicts of interest

There are no conflict to declare.

Acknowledgements

This study was supported by UNSW Vice-Chancellor's Research Fellowship for Y. Xue. C. Jia acknowledges funding from the National Natural Science Foundation of China (51572109) and Shandong Provincial Natural Science Foundation (ZR2015EL008), and Graduate Innovation Foundation of University of Jinan (GIFUJN YCXB15002).

Notes and references

1 M. Aono and K. Ariga, *Adv. Mater.*, 2016, **28**, 989.
2 V. Malgras, Q. Ji, Y. Kamachi, T. Mori, F.-K. Shieh, K. C.-W. Wu, K. Ariga and Y. Yamauchi, *Bull. Chem. Soc. Jpn.*, 2015, **88**, 1171.
3 D. Chen, H. Zhang, Y. Liua and J. Li, *Energy Environ. Sci.*, 2013, **6**, 1362.
4 K. S. Novoselov, A. K. Geim, S. V. Morozov, D. Jiang, Y. Zhang, S. V. Dubonos, I. V. Grigorieva and A. A. Firsov, *Science*, 2004, **306**, 666.
5 H. Chen, M. B. Miller, K. J. Gilmore, G. G. Wallace and D. Li, *Adv. Mater.*, 2008, **20**, 3557.
6 F. He, G. Chen, J. Miao, Z. Wang, D. Su, S. Liu, W. Cai, L. Zhang, S. Hao and B. Liu, *ACS Energy Lett.*, 2016, **1**, 969.
7 X. Wang, K. Maeda, A. Thomas, K. Takanabe, G. Xin, J. M. Carlsson, K. Domen and M. Antonietti, *Nat. Mater.*, 2009, **8**, 76.
8 A. K. Geim and K. S. Novoselov, *Nat. Mater.*, 2007, **6**, 183.
9 X. Wang, K. Maeda, X. Chen, K. Takanabe, K. Domen, Y. Hou, X. Fu and M. Antonietti, *J. Am. Chem. Soc.*, 2009, **131**, 1680.
10 K. Kailasam, J. D. Epping, A. Thomas, S. Losse and H. Junge, *Energy Environ. Sci.*, 2011, **4**, 4668.
11 S. C. Yan, Z. S. Li and Z. G. Zou, *Langmuir*, 2009, **25**, 10397.
12 H. Yan, *Chem. Commun.*, 2012, **48**, 3430.
13 L. Ge, C. Hanb and J. Liu, *J. Mater. Chem.*, 2012, **22**, 11843.
14 J.-S. Shen, Q.-G. Cai, Y.-B. Jiang and H.-W. Zhang, *Chem. Commun.*, 2010, **46**, 6786.
15 J. H. Wei, Q. Zhang, Y. Liu, R. Xiong, C. X. Pan and J. Shi, *J. Nanopart. Res.*, 2011, **13**, 3157.
16 D. C. Marcano, D. V. Kosynkin, J. M. Berlin, A. Sinitskii, Z. Sun, A. Slesarev, L. B. Alemany, W. Lu and J. M. Tour, *ACS Nano*, 2010, **4**, 4806.
17 Y. Xue, Y. Liu, F. Lu, J. Qu, H. Chen and L. Dai, *J. Phys. Chem. Lett.*, 2012, **3**, 1607–1612.
18 Y. Liu, X. Zhang, J. Wang and P. Yang, *RSC Adv.*, 2016, **6**, 112581.
19 Y. Liu, X. Zhang, J. Wang and P. Yang, *Phys. Chem. Chem. Phys.*, 2016, **18**, 31513.
20 A. Thomas, A. Fischer, F. Goettmann, M. Antonietti, J. O. Müller, R. Schlog and J. M. Carlsson, *J. Mater. Chem.*, 2008, **18**, 4893.
21 J. Li, L. H. Zhu, Y. H. Wu, Y. Harima, A. Q. Zhang and H. Q. Tang, *Polymer*, 2006, **47**, 7361.
22 Y. Liu, J. Wang and P. Yang, *RSC Adv.*, 2015, **5**, 61657.
23 J. Liu, Y. Liu, N. Y. Liu, Y. Z. Han, X. Zhang, H. Huang, Y. Lifshitz, S. T. Lee, J. Zhong and Z. H. Kang, *Science*, 2015, **347**, 970.
24 Q. Z. Yu, M. Wang, H. Z. Chen and Z. W. Dai, *Mater. Chem. Phys.*, 2011, **129**, 666.
25 H. Zhang and Y. F. Zhu, *J. Phys. Chem. C*, 2010, **114**, 5822.